https://doi.org/10.20965/ijat.2019.p0671

Paper:

Generation of a High-Precision Digital Elevation Model for Fields in Mountain Regions Using RTK-GPS

Liangliang Yang[*,†], Hao Guo[**], Shuming Yang[**], Yohei Hoshino[*], Soichiro Suzuki[*], Dehua Gao[**], and Ying Cao[*]

[*]Kitami Institute of Technology
165 Koen-cho, Kitami-shi, Hokkaido 090-8507, Japan
[†]Corresponding author, E-mail: yang@mail.kitami-it.ac.jp
[**]Ningxia University, Yinchuan, China
[Received November 7, 2017; accepted June 29, 2019]

In modern agriculture, many advanced automated devices are used on farms. To improve the working efficiency of agricultural vehicles, fields are expected to be pre-leveled, because the vehicles work more effectively on a flat field. Leveling a field requires the current field elevation map. Some farmers in Japan have begun to use high-precision real-time kinematic Global Positioning System (RTK-GPS)-based self-steering tractors in the fields. This study uses the RTK-GPS information from a self-steering tractor system to generate a digital elevation model (DEM) especially in mountain regions where the fields are not flat. In addition, all of the information is from the self-steering system with the result that farmers can use the method of this study without additional instruments. However, the GPS receiver sometimes cannot obtain high-quality signals from satellites in mountain regions. Therefore, this study focuses on how to create a high-precision DEM even when a GPS signal is unavailable. It proposes a dynamic interpolation method for generating a DEM. In addition, a test was conducted in a field in a mountain region. The test results show that the dynamic interpolation method can provide an accuracy of less than 0.03 m in the test field for creating a DEM.

Keywords: DEM, RTK-GPS, high precision, mountain regions, dynamic interpolation

1. Introduction

Three-dimensional (3D) information is important for indoor modern robot control [1], 3D printing [2], and outdoor robot navigation [3, 4]. For wider-area applications, a 3D model was used to inspect the aging of bridges [5], detect target persons [6], and represent the surface shape of the terrain [7]. An airborne device with a laser altimeter has been used to generate a digital elevation model (DEM) [8]. The accuracy of the laser altimeter is between 0.1 m and 0.12 m. Such accuracy is fine for surveying, but some applications require a higher accuracy; for example, mm-level accuracy terrestrial laser scanners (TLSs) have been used in civil engineering [9, 10]. Obtaining high-accuracy data using TLSs always requires fixing settings on a point when scanning without moving. Therefore, a TLS is not typically used for large area DEM scanning.

For moving applications, Gamba and Houshmand [11] compared the data from interferometric synthetic aperture radar (IFSAR) and Light Detection and Ranging (LiDAR) for obtaining the 3D shape of a field, with results showing that LiDAR is better than IFSAR for large outdoor use. The LiDAR system was used for large areas with its advantage of high accuracy, for example, for documenting floods [12, 13] and for assessing rock glaciers and glaciers [14]. Dehvari and Heck [15] analyzed the accuracy difference between photo-based and LiDAR DEMs, with results showing that the vertical accuracy was approximately 0.3 m and 0.2 m for the photo-based and LiDAR DEMs, respectively. The accuracy was sufficiently high for understanding the surface shape of the field. However, in the application using LiDAR, the data for some areas always either could not be scanned and/or contained noise points. A study was conducted on smoothing LiDAR data [16] by using a threshold to filter out the noise points whose heights differ from the average height of a selected area.

However, because the LiDAR system was typically used in an airborne surveying system, the DEM accuracy was at m-level and not the expected cm-level [17]. Improving the accuracy of the DEM required reducing the scanning area and interpolating to refine the raw LiDAR data. Natural neighbor (NN) has proved to be effective for DEM generation [18, 19]. The best result obtained in the study with NN interpolation at 50% decimation was approximately 0.1 m. The higher the spatial resolution of the DEM, the better people can analyze the earth's surface condition. This is very useful for agriculture, because both field and crop conditions are expected be monitored [20, 21]. Therefore, an unmanned aerial vehicle (UAV) has been used to obtain the DEM [22], and the DEM time series were used to locate and quantify erosion and deposition in a context of an agricultural watershed with silt loam soils and a smooth relief. In addition, to

Fig. 1. Experiment vehicle with the RTK-GPS.

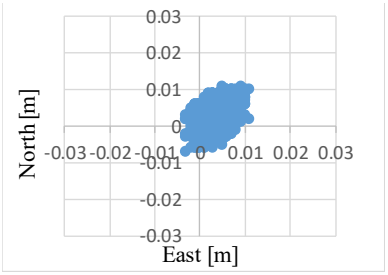

(a)

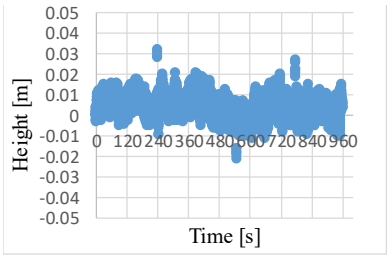

(b)

Fig. 2. Accuracy of the RTK-GPS (a) horizontal (b) vertical direction.

obtain a high-precision DEM of the field to analyze information such as yield, a vehicle-mounted high-resolution LiDAR (0.1 m accuracy) and low accuracy GPS system were used [23]. The results show that the LiDAR data are usable while the GPS data were not suitable. There is a high precision RTK-GPS (0.03 m accuracy) available today. It has the potential to be used to generate a high-precision DEM. Therefore, in this study, a high precision (cm-level) DEM is generated using an RTK-GPS instead of LiDAR. Moreover, a projection method of the raw data from the RTK-GPS to the real ground and interpolation of the gapped area method are also introduced.

2. Experimental Equipment and Method

As shown in **Fig. 1**, a wheel-type tractor was used as a moving vehicle platform to obtain raw GPS data. An RTK-GPS (GR2100, Topcon, USA) was installed inside the cabin, and an antenna for the GPS receiver was mounted above the implement of the tractor.

The precision of the RTK-GPS is shown in **Fig. 2** for the horizontal and vertical directions, respectively. The

Fig. 3. Field for experiment in the mountain region.

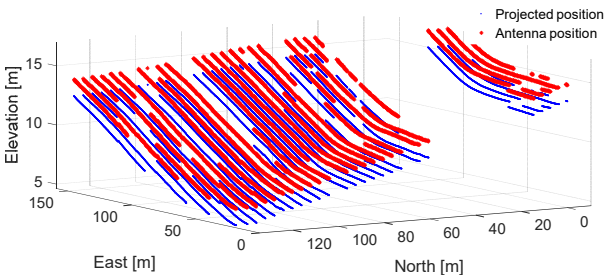

Fig. 4. Position of the GPS and the position after being projected to the ground surface.

data were acquired in outdoor conditions on a sunny day.

The precision of the horizontal direction is less than ± 0.02 m in both the east and north directions, and the vertical direction is less than ± 0.03 m. In addition, an inertial measurement unit (IMU) was installed under the GPS antenna to measure the inclination of the implement.

3. Dynamic Interpolation and DEM Generation

The experiment of this study was conducted in a field located in a mountain region. **Fig. 3** illustrates the field condition. The raw data from the GPS and IMU were logged at 10 Hz during the planting operation using the tractor.

3.1. Projecting the GPS Data from the Antenna Position to the Ground Surface

The GPS and IMU data were processed in the office in off time rather than in the field. The time stamps of the GPS and IMU data were used to synchronize the data. As shown in **Fig. 1**, the GPS antenna was installed above the implement. However, the DEM of the field surface was to be generated. Therefore, first, the points measured by the GPS had to be projected to the ground surface. As shown in **Fig. 4**, the red asterisks are the raw data taken directly from the GPS antenna position. Only the high-precision data are shown in **Fig. 4**. The gap in the data is the area in which the RTK-GPS could not obtain a fix-solution because of the lack of signal from satellites and/or the base station. The blue dots are the positions that were projected

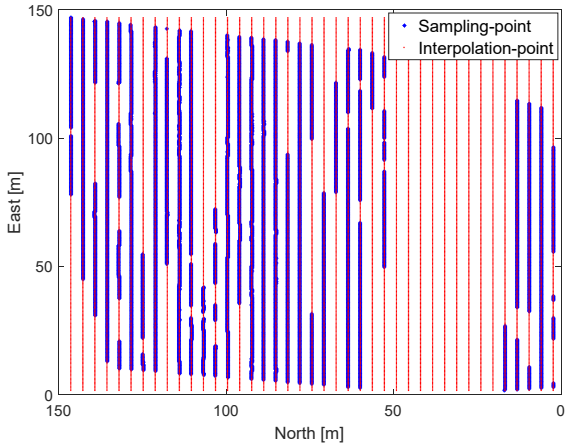

Fig. 5. Interpolation points of the field.

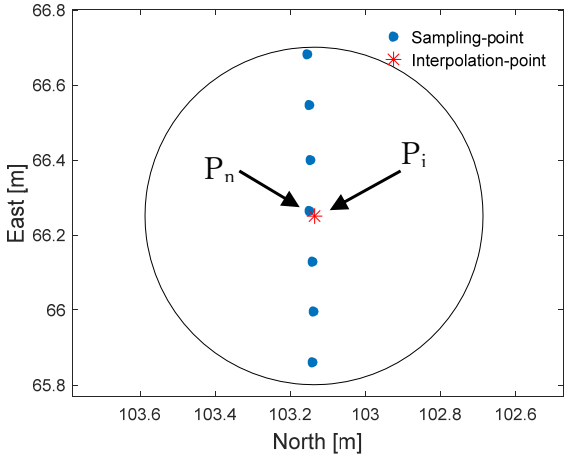

Fig. 6. Replace the interpolation point by the nearest point within 0.3 m.

to the ground surface using Eq. (1).

$$\begin{bmatrix} P_{ie} \\ P_{in} \\ P_{iu} \end{bmatrix} = \begin{bmatrix} P_{ge} \\ P_{gn} \\ P_{gu} \end{bmatrix} - \mathbf{R} \begin{bmatrix} 0 \\ 0 \\ h \end{bmatrix} \quad \ldots\ldots \quad (1)$$

where $\mathbf{R} = \mathbf{R_z R_y R_x}$,

$$\mathbf{R_x} = \begin{bmatrix} 1 & 0 & 0 \\ 0 & C_\psi & -S_\psi \\ 0 & S_\psi & C_\psi \end{bmatrix}, \quad \mathbf{R_y} = \begin{bmatrix} C_\theta & 0 & S_\theta \\ 0 & 1 & 0 \\ -S_\theta & 0 & C_\theta \end{bmatrix},$$

$$\mathbf{R_z} = \begin{bmatrix} C_\phi & -S_\phi & 0 \\ S_\phi & C_\phi & 0 \\ 0 & 0 & 1 \end{bmatrix}.$$

C and S refer to the cos and sin operators respectively, and ψ, θ, and ϕ are the respective Euler angles to the X-, Y-, and Z-axes of the vehicle coordinates; X-points are to the right side of the vehicle, Y-points are to the front of the vehicle, and Z-points are up following the right-hand rule; $[0,0,h]^T$ is the coordinate value of the GPS antenna in the vehicle coordinates. P_{ie}, P_{in}, and P_{iu} are the coordinate values of the projected position in east, north, and up direction, respectively. P_{ge}, P_{gn}, and P_{gu} are the coordinate values of the raw position in the east, north, and up direction from the GPS antenna.

3.2. Dynamic Interpolation Method to Fill the Gap in the GPS Data

The working swath of the vehicle can be in any direction. To normalize the interpolation method, as shown in **Fig. 5**, the sampling point data that projected to the ground were rotated to the up-down direction. This ensures that each row of the sampling point cloud data is parallel to the east-axis in the local coordinate system. The distance between two neighbor swaths is 3.6 m, and the distance between the points in one swath is less than 0.2 m.

Figure 5 shows the interpolating points in red and the sampling points from **Fig. 4**. The blue asterisks are sampling points in **Fig. 5**. The interpolating points in **Fig. 5** are grid points of the field.

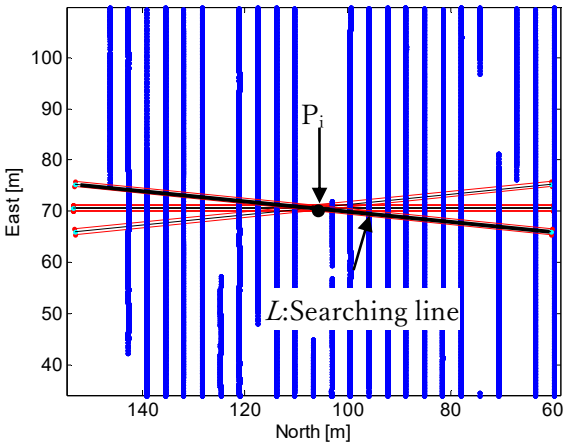

Fig. 7. Dynamic searching interpolation.

The dynamic interpolation method includes three steps as follows.

First step (*replacement step*): as shown in **Fig. 6**, if there is a sampling point P_n near the interpolation point P_i with a range of 0.3 m, replace the interpolation point with the nearest sampling point. Otherwise, go to the second step.

Second step (*dynamic searching step*): as shown in **Fig. 7**, if the interpolation point P_i is at a position at which there is a big gap in the swath, it is difficult to interpolate the points using only the neighborhood points. It is for this reason that a dynamic searching interpolation method was proposed to fill the big gap. In **Fig. 7**, P_i is the point that will be interpolated, and L is the dynamic searching line.

The meaning of *dynamic* in the searching step is that 1) the direction and 2) the length of the searching line are dynamically changed. In **Fig. 7**, the interpolation point P_i is the center of line L. The width of L is 1 m, and the length of L is changed so that at least ten sampling points can be searched by L on both sides of P_i. The slope of the searching L is changed from the horizontal direction by

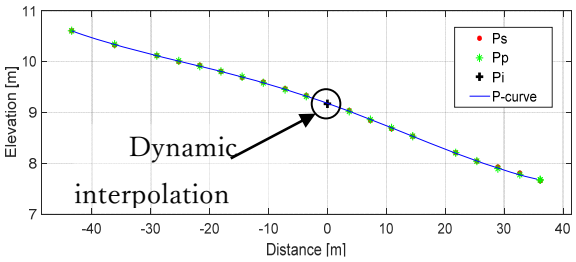

Fig. 8. Polynomial fitting interpolation.

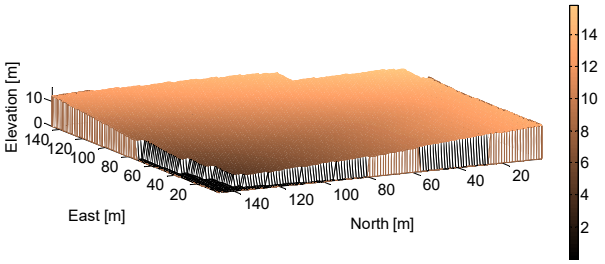

Fig. 9. DEM using the dynamic interpolation method.

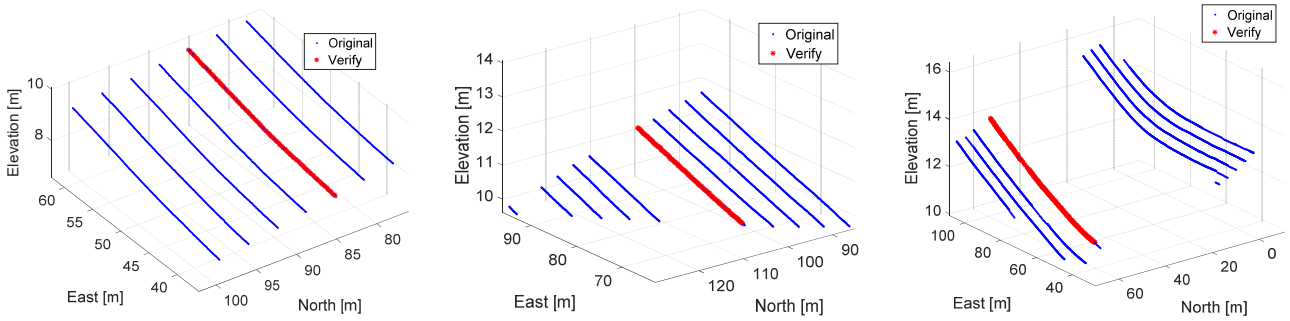

Fig. 10. Three typical types of interpolation region for verification.

steps of $1/10$ until all the sampling data have been covered. The direction that can cover the most of the sampling data is selected as the interpolation direction. There will be a series of points along the selected searching line defined as $P_s(n)$, where the subscript n is the serial number of the points.

Third step (*dynamic interpolation step*): a polynomial fitting method was used to calculate the elevation of P_i using the searched points $P_s(n)$ using Eq. (2),

$$z = m \cdot x^n + \cdots + a \cdot x^3 + b \cdot x^2 + c \cdot x + z_0 \quad . \quad . \quad . \quad (2)$$

where x is the distance from sampling point $P_s(n)$ to interpolation point P_i, and z is the elevation of the corresponding point. n is the highest order of the polynomial function, which is set to less than five. In practice, n will improve from two to five if the fitting accuracy is larger than 0.05 m. The fitted function using the least squares method of the curve in **Fig. 8** is Eq. (3) when n is 4,

$$y = 0.00000014527 \cdot x^4 + 0.000003126 \cdot x^3 - 0.00032179 \cdot x^2 - 0.040887 \cdot x + 9.176. \quad (3)$$

In **Fig. 8**, the red points are the sampling points P_s, the green asterisks P_p are the interpolated points, the blue curve (P-curve) illustrates Eq. (3), the dynamic interpolation point P_i is shown in black crosses, the horizontal coordinate value is zero, and the vertical coordinate value is 9.18 m, the elevation of the interpolated point. **Fig. 9** shows the DEM generated using the interpolated data calculated using the proposed method. The DEM was shown using MATLAB software.

4. Results and Discussion

Three typical types of verification region (**Fig. 10**) were selected to verify the accuracy of the interpolation method for creating a DEM using RTK-GPS. The first type of region, the double-sided pre-known (DSP) region (**Fig. 10(a)**), is used when there are pre-known position and elevation data from the RTK-GPS receiver on both sides of neighboring paths. The second type of region (**Fig. 10(b)**), the single-sided pre-known (SSP) region, is used when there are pre-known position and elevation data on only one side of the neighboring swath. The third type of region (**Fig. 10(c)**), the no pre-known (NP) region, is used when there are no pre-known position and elevation data in the neighboring paths. The blue points are the original points and the red asterisks are verification points in **Fig. 10**. In addition, three types of interpolation methods (triangle lineal, triangle cubic, and nearest neighbor) have been used for interpolation of the elevation data for comparison. **Fig. 11** shows the triangle interpolation net for both the triangle lineal and triangle cubic methods.

The red points P_i in **Fig. 11** are the interpolation points, and the blue points P_s are the sampling points. The triangle lineal method uses the interpolation function Eq. (4).

$$z_i = z_1 \cdot W_1 + z_2 \cdot W_2 + z_3 \cdot W_3 \quad . \quad . \quad . \quad . \quad . \quad . \quad . \quad (4)$$

where

$$W_1 = \frac{(x_2 - x_i) \cdot (y_3 - y_i) - (x_3 - x_i) \cdot (y_2 - y_i)}{M},$$

$$W_2 = \frac{(x_3 - x_i) \cdot (y_1 - y_i) - (x_1 - x_i) \cdot (y_3 - y_i)}{M},$$

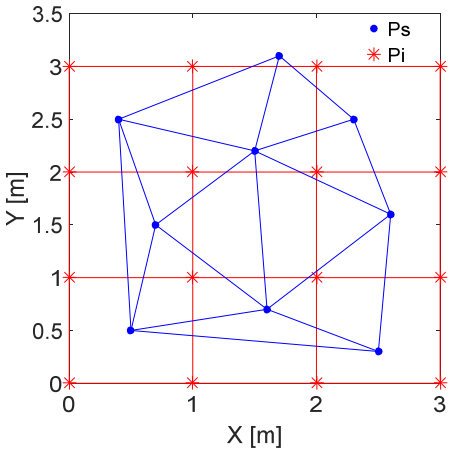

Fig. 11. Triangle lineal interpolation method.

$$W_3 = \frac{(x_1 - x_i)\cdot(y_2 - y_i) - (x_2 - x_i)\cdot(y_1 - y_i)}{M},$$
$$M = (x_2 - x_1)\cdot(y_3 - y_1) - (x_3 - x_1)\cdot(y_2 - y_1).$$

The triangle cubic method uses the interpolation function Eq. (5),

$$A(x_i - x_1) + B(y_i - y_1) + C(z_i - z_1) = 0 \quad . \quad . \quad . \quad (5)$$

where x, y, and z are the coordinates of the points, the subscript i indicates the interpolation points, and the subscript one, two, and three indicate the three vertices of the triangle,

$$A = (y_3 - y_1)\cdot(z_3 - z_1) - (z_2 - z_1)\cdot(y_3 - y_1),$$
$$B = (x_3 - x_1)\cdot(z_2 - z_1) - (x_2 - x_1)\cdot(z_3 - z_1),$$
$$C = (x_2 - x_1)\cdot(y_3 - y_1) - (x_3 - x_1)\cdot(y_2 - y_1).$$

In addition, the nearest neighbor method takes the elevation of the interpolation point to be the elevation of the nearest point to the interpolation point. This is the simplest method.

Figures 12 and **13** show the interpolation error using the triangle cubic (red curve), triangle lineal (black curve), dynamic (blue curve), and nearest neighbor method calculated using Eq. (6),

$$e_i = z_i - r_i, \quad (i = 1, 2, 3, \ldots, N) \quad . \quad . \quad . \quad . \quad . \quad . \quad (6)$$

where z_i is the interpolated elevation, r_i is the elevation of the verification points, e_i is the interpolation error, and the subscript i is the index of the verification points.

From **Fig. 12** it can be seen that the dynamic interpolation method of this paper provides the smallest error of less than 0.03 m in all three verification regions. In addition, the maximum error for the DSP region using the cubic and triangle lineal methods is approximately 0.06 m while that of the dynamic method is less than 0.03 m. The maximum error for the SSP and NP of the dynamic method are also less than those of the other methods.

Figure 13 shows the error using the nearest neighbor method for the DSP, SSP, and NP regions. It can be seen that in any of the conditions the error is larger than 0.1 m,

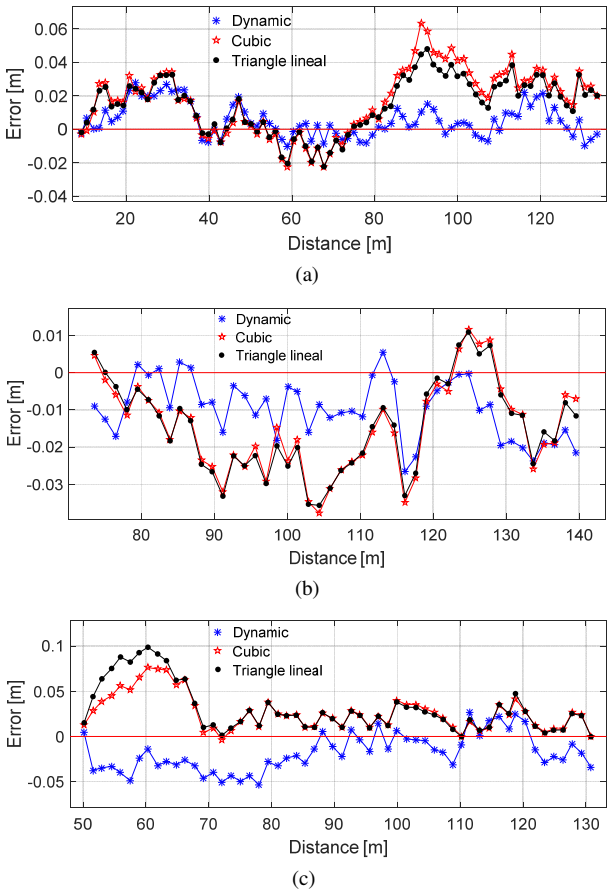

Fig. 12. Interpolation error using triangle lineal (black), cubic (red) and dynamic (blue) methods.

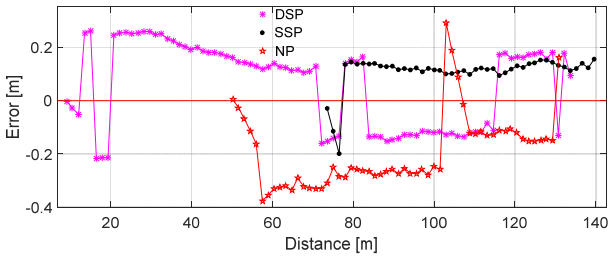

Fig. 13. Interpolation error using nearest neighbor in DSP, SSP, and NP.

and even near 0.4 m for the NP region. Consequently, the nearest neighbor method is not suitable for high-precision DEM generation.

Table 1 shows the root mean square (RMS) value of the interpolation accuracy of the various interpolation methods.

The dynamic interpolation method provides the highest interpolation accuracy, while the nearest neighbor method provides the lowest interpolation accuracy in all of the verification regions. In addition, the accuracy of the triangle cubic and triangle lineal methods are nearly the same for the three types of verification regions. Moreover, the interpolation error is less than 0.03 m in all three verification regions when using the dynamic interpola-

Table 1. Accuracy of the different interpolation methods.

Interpolation method	RMS [m]		
	DSP region	SSP region	NP region
Dynamic	0.011	0.012	0.027
Triangle cubic	0.026	0.019	0.033
Triangle lineal	0.022	0.019	0.040
Nearest neighbor	0.168	0.126	0.236

tion method.

The reason why dynamic method can give better interpolation accuracy is that it has the advantage of using a nonlinear curve to fit the points, in addition, a dynamic searching area was set to search more possible data instead of using neighbor data only like other three algorithms.

5. Conclusions

A high precision RTK-GPS was used for generation of a DEM for agriculture in mountain regions. Because the RTK-GPS cannot provide the FIX-solution data in some conditions when the signal from the satellites and/or base station could not be received, an interpolation method is required to interpolate the gap area of the field. In this study, a dynamic interpolation method was proposed, and the method was verified in three types of region. The first type is when there are sampling points on both sides of the interpolation points; the second type is when there are sampling points on one side of the interpolation points; the third type is when there are no sampling points near the interpolation points. Compared with the triangle cubic, triangle lineal, and nearest neighbor methods, the dynamic interpolation method provided the best interpolation results for three types of region. The accuracies were 0.011 m, 0.012 m, and 0.027 m for the first, second, and third type of regions, respectively. The method can be used to generate a high accuracy DEM using only RTK-GPS.

References:

[1] K. Hoshino and K. Hamamatsu, "Three-Dimensional Input System Employing Pinching Gestures for Robot Design," Int. J. Automation Technol., Vol.11, No.3, pp. 378-384, 2017.

[2] K. Kawagishi, S. Umetani, K. Tanaka, E. Ametani, Y. Morimoto, and K. Takasugi, "Development of Four-Axis 3D Printer with Fused Deposition Modeling Technology," Int. J. Automation Technol., Vol.11, No.2, pp. 278-286, 2017.

[3] H. Tsukagoshi, N. Arai, I. Kiryu, and A. Kitagawa, "Tip Growing Actuator with the Hose-Like Structure Aiming for Inspection on Narrow Terrain," Int. J. Automation Technol., Vol.5, No.4, pp. 516-522, 2017.

[4] L. Bruzzone, P. Fanghella, and G. Quaglia, "Experimental Performance Assessment of Mantis 2, Hybrid Leg-Wheel Mobile Robot," Int. J. Automation Technol., Vol.11, No.3, pp. 396-403, 2017.

[5] Y. Hada, M. Nakao, M. Yamada, H. Kobayashi, N. Sawasaki, K. Yokoji, S. Kanai, F. Tanaka, H. Date, S. Pathak, A. Yamashita, M. Yamada, and T. Sugawara, "Development of a Bridge Inspection Support System Using Two-Wheeled Multicopter and 3D Modeling Technology," J. Disaster Res., Vol.12, No.3, pp. 593-606, 2017.

[6] K. Hosaka and T. Tomizawa, "A Person Detection Method Using 3D Laser Scanner – Proposal of Efficient Grouping Method of Point Cloud Data," J. Robot. Mechatron., Vol.27, No.4, pp. 374-381, 2015.

[7] R. Takemura and G. Ishigami, "Traversability-Based RRT* for Planetary Rover Path Planning in Rough Terrain with LIDAR Point Cloud Data," J. Robot. Mechatron., Vol.29, No.5, pp. 838-846, 2017.

[8] J. L. Bamber, S. Ekholm, and W. B. Krabill, "A New, High-Resolution Digital Elevation Model of Greenland Fully Validated with Airborne Laser Altimeter Data," J. of Geophysical Research: Solid Earth, Vol.106, No.B4, pp. 6733-6745, 2001.

[9] M. Pejić, V. Ogrizović, B. Božić, B. Milovanović, and S. Marošan, "A Simplified Procedure of Metrological Testing of the Terrestrial Laser Scanners," Measurement, Vol.53, pp. 260-269, 2014.

[10] P. Hartzell, C. Glennie, K. Biber, and S. Khan, "Application of Multispectral LiDAR to Automated Virtual Outcrop Geology," ISPRS J. of Photogrammetry and Remote Sensing, Vol.88, pp. 147-155, 2014.

[11] P. Gamba and B. Houshmand, "Digital Surface Models and Building Extraction: A Comparison of IFSAR and LIDAR Data," IEEE Trans. on Geoscience and Remote Sensing, Vol.38, No.4, pp. 1959-1968, 2000.

[12] B. Chen, W. F. Krajewski, R. Goska, and N. Young, "Using LiDAR surveys to document floods: A case study of the 2008 Iowa flood," J. of Hydrology, Vol.553, pp. 338-349, 2017.

[13] B. B. Shrestha, H. Sawano, M. Ohara, and N. Nagumo, "Improvement in Flood Disaster Damage Assessment Using Highly Accurate IfSAR DEM," J. Disaster Res., Vol.11, No.6, pp. 1137-1149, 2016.

[14] J. R. Janke, "Using Airborne LiDAR and USGS DEM Data for Assessing Rock Glaciers and Glaciers," Geomorphology, Vol.195, pp. 118-130, 2013.

[15] A. Dehvari and R. J. Heck, "Removing Non-Ground Points from Automated Photo-Based DEM and Evaluation of its Accuracy with LiDAR DEM," Computers & Geosciences, Vol.43, pp. 108-117, 2012.

[16] S. Li, R. A. MacMillan, D. A. Lobb, B. G. McConkey, A. Moulin, and W. R. Fraser, "Lidar DEM error analyses and topographic depression identification in a hummocky landscape in the prairie region of Canada," Geomorphology, Vol.129, Nos.3-4, pp. 263-275, 2011.

[17] R. M. Langridge, W. F. Ries, T. Farrier, N. C. Barth, N. Khajavi, and G. P. De Pascale, "Developing sub 5-m LiDAR DEMs for forested sections of the Alpine and Hope faults, South Island, New Zealand: Implications for structural interpretations," J. of Structural Geology, Vol.64, pp. 53-66, 2014.

[18] M. P. Smith, A-X. Zhu, J. E. Burt, and C. Stiles, "The Effects of DEM Resolution and Neighborhood Size on Digital Soil Survey," Geoderma, Vol.137, Nos.1-2, pp. 58-69, 2006.

[19] N. Polat, M. Uysal, and A. S. Toprak, "An Investigation of DEM Generation Process based on LiDAR Data Filtering, Decimation, and Interpolation Methods for an Urban Area," Measurement, Vol.75, pp. 50-56, 2015.

[20] M. Mokarram and M. Hojati, "Morphometric Analysis of Stream as One of Resources for Agricultural Lands Irrigation Using High Spatial Resolution of Digital Elevation Model (DEM)," Computers and Electronics in Agriculture, Vol.142, Part A, pp. 190-200, 2017.

[21] I. A. Thomas, P. Jordan, O. Shine, O. Fenton, P. E. Mellander, P. Dunlop, and P. N. C. Murphy, "Defining Optimal DEM Resolutions and Point Densities for Modelling Hydrologically Sensitive Areas in Agricultural Catchments Dominated by Microtopography," Int. J. of Applied Earth Observation and Geoinformation, Vol.54, pp. 38-52, 2017.

[22] N. Pineux, J. Lisein, G. Swerts, C. L. Bielders, P. Lejeune, G. Colinet, and A. Degré, "Can DEM time Series Produced by UAV be used to Quantify Diffuse Erosion in an Agricultural Watershed?," Geomorphology, Vol.280, pp. 122-136, 2017.

[23] J. M. McKinion, J. L. Willers, and J. N. Jenkins, "Comparing high density LIDAR and medium resolution GPS generated elevation data for predicting yield stability," Computers and Electronics in Agriculture, Vol.74, No.2, pp. 244-249, 2010.

Name:
Liangliang Yang

Affiliation:
Kitami Institute of Technology

Address:
165 Koen-cho, Kitami-shi, Hokkaido 090-8507, Japan

Brief Biographical History:
2013- Postdoctoral Researcher, Hokkaido University
2015- Assistant Professor, Kitami Institute of Technology

Main Works:
• "Development of a Crawler-type Robot Tractor Using RTK-GPS and IMU," Engineering in Agriculture, Environment and Food, Vol.7, No.4, pp. 143-147, 2014.
• "Development and Application of a Wheel-type Robot Tractor," Engineering in Agriculture, Environment and Food, Vol.9, No.2, pp. 131-140, 2016.
• "Leader-follower System Using Two Robot Tractors to Improve Work Efficiency," Computers and Electronics in Agriculture, Vol.121, pp. 269-281, 2016.

Membership in Academic Societies:
• Robotics Society of Japan (RSJ)
• Japanese Society of Agricultural Machinery and Food Engineers (JSAM)

Name:
Hao Guo

Affiliation:
Hardware in Loop (HIL) Test Engineer, Great Wall Motor Company Limited

Address:
No.67 EastSheng Road, Great Wall Transmission Academe, Baoding, Hebei 071000, China

Brief Biographical History:
2016 Received Master's degree from Ningxia University
2017- Visiting Student, Department of Mechanical Engineering, Kitami Institute of Technology
2019- Hardware in Loop (HIL) Test Engineer, Great Wall Motor Company Limited

Main Works:
• HIL testing for EPS ECU

Name:
Shuming Yang

Affiliation:
Professor, School of Mechanical Engineering, Ningxia University

Address:
No.539 Helanshan West Road, Xixia District, Yinchuan, Ningxia Hui Autonomous Region 750021, China

Brief Biographical History:
1998- Ningxia Agricultural College
2002- Ningxia University
2005 Received Ph.D. from Northwest A&F University

Main Works:
• "Design and experimental validation of improved grapevine burying machine," Int. J. Agric. & Biol. Eng., Vol.11, pp. 95-100, 2018.
• "Mathematic Models of Water Application for a Variable Rate Irrigating Hill-seeder," Trans. of the CSAM, Vol.40, pp. 41-44, 2009.

Membership in Academic Societies:
• Chinese Society of Agricultural Engineering (CSAE)

Name:
Yohei Hoshino

Affiliation:
Kitami Institute of Technology

Address:
165 Koen-cho, Kitami-shi, Hokkaido 090-8507, Japan

Brief Biographical History:
2004- Research Associate, Graduate School of Engineering, Hokkaido University
2007- Assistant Professor, Graduate School of Engineering, Hokkaido University
2010- Assistant Professor, Faculty of Engineering, Hokkaido University
2013- Assistant Professor, Department of Mechanical Engineering, Kitami Institute of Technology
2014- Associate Professor, Department of Mechanical Engineering, Kitami Institute of Technology
2019- Professor, Group of Mechanical-Electrical Engineering, Kitami Institute of Technology

Main Works:
• "Force Redistribution Method for Compensating Actuator-Breakdown of Vibration-Isolation Tables Supported with a Redundant Number of Pneumatic Actuators," J. of System Design and Dynamics, Vol.7, No.4, pp. 355-366, 2013.
• "Self-Identification Method of Arrangement and Effective Pressure Areas for a Vibration-Isolation Table Supported with a Redundant Number of Pneumatic Actuators," JSME Mechanical Engineering J., Vol.2, No.3, pp. 1-11, 2015.
• "Cost-Performance Enhancement of an Active Wheel Damper for Flexible Structures by Using the Dynamic Quantizer," Trans. of the JSME, Vol.82, No.837, 15-00652, 2016.

Membership in Academic Societies:
• Japan Society of Mechanical Engineers (JSME)
• Robotics Society of Japan (RSJ)
• Society of Instrument and Control Engineers (SICE)
• Japanese Society of Agricultural Machinery and Food Engineers (JSAM)

Name:
Soichiro Suzuki

Affiliation:
Kitami Institute of Technology

Address:
165 Koen-cho, Kitami-shi, Hokkaido 090-8507, Japan

Brief Biographical History:
1984- Research Institute of Sports Science, Asics Corporation
1993- Assistant Professor, Department of Mechanical System Engineering, Kitami Institute of Technology
1999- Associate Professor, Department of Mechanical System Engineering, Kitami Institute of Technology
2011- Professor, Department of Mechanical Engineering, Kitami Institute of Technology

Main Works:
- "Development of an autonomous snow plow robot utilizing RTK-GPS," GIS·GPS Report, Vol.1, p. 35, 2007.
- "Analysis of the skill of a world-class alpine ski racer by using a 3D CAD system," The Int. J. of Engineering and Science, Vol.5, pp. 34-37, 2016.
- "Fundamental study of a sports motion analysis system by using DNN," The Proc. of the Symp. on Sports and Human Dynamics, C-30, 2018.

Membership in Academic Societies:
- Japan Society of Mechanical Engineers (JSME)

Name:
Dehua Gao

Affiliation:
School of Mechanical Engineering, Ningxia University

Address:
No.539 Helanshan West Road, Xixia District, Yinchuan, Ningxia Hui Autonomous Region 750021, China

Brief Biographical History:
2015- Postgraduate Student, Ningxia University
2018 Received Ph.D. from China Agriculture University

Main Works:
- Agricultural intelligent instrument, spectral analysis

Membership in Academic Societies:
- Chinese Society of Agricultural Engineering (CSAE)

Name:
Ying Cao

Affiliation:
Kitami Institute of Technology

Address:
165 Koen-cho, Kitami-shi, Hokkaido 090-8507, Japan

Brief Biographical History:
2015- Kitami Institute of Technology

Main Works:
- "Turn Control of a Three-Dimensional Quasi-Passive Walking Robot by Utilizing a Mechanical Oscillator," Engineering, Vol.6, No.2, pp. 93-99, 2014.
- "Uphill and level walking of a three-dimensional biped quasi-passive walking robot by torso control," Robotica, Vol.34, pp. 483-496, 2016.

Membership in Academic Societies:
- Japan Society of Mechanical Engineers (JSME)
- Robotics Society of Japan (RSJ)